Structural Eng./Earthquake Eng., JSCE, Vol. 19, No. 2 [Special Issue], 209s—219s, 2002 October

DEFORMATION OF SANDY DEPOSITS BY REVERSE FAULTING

Hisashi TANIYAMA[1] and Hiroyuki WATANABE[2]

[1]Member of JSCE, Dr. Eng., Research Assoc., Dept. of Civil and Environmental Eng., Saitama University
(255 Shimo-Okubo, Saitama-shi, Saitama 338-8570, Japan)
[2]Member of JSCE, Dr. Eng., Professor, Dept. of Civil and Environmental Eng., Saitama University
(255 Shimo-Okubo, Saitama-shi, Saitama 338-8570, Japan)

We performed sandbox tests and numerical analysis of the tests to investigate the deformation of the sand by reverse faulting. Test results can be simulated generally well by FEM using elasto-plastic solid elements and joint elements, if the stress-strain relation of the sand is adequately modeled. We applied our numerical model to prototypic real scale sandy alluvium model. The analyses of 30m, 50m and 75m deep alluvium suggested that the failure surface propagates through the alluvium if the vertical bedrock fault displacement reaches 3-7% of the depth of the alluvium. It is unlikely that the shear failure propagates through 100m deep alluvium.

Key Words : *earthquake fault, reverse fault, deposits, elato-plastic analysis, FEM*

1. INTRODUCTION

The understanding of earthquake fault rupture propagation through unconsolidated deposits overlying potentially active faults is important in planning structures near such faults. It is also important for mid term to long term earthquake prediction because recurrence period of earthquakes is often inferred by surface-faulting earthquakes.

Cole and Lade[1] performed tests using dry sand and predicted the shape of the failure surface over dip-slip fault as a function of the depth of the soil, the angle of dilation for the soil, and the dip angle of the fault. Tani and Ueta[2] modified Cole and Lade's formulation from the kinematic point of view.

Scott and Schoustra[3] performed numerical simulation of 800m-deep alluvium over vertical fault by two-dimensional finite element method (FEM) assuming a linear-perfectly plastic relation. Their results showed the rupture zone bending over to the upthrown side, which is not consistent with experimental results. Roth et al.[4] compared the centrifuge tests and the shear rupture in 6m deposits with their finite difference simulation and concluded the simulation could duplicate the experiments qualitatively.

Walters and Thomas[5] performed sandbox experiment and conducted numerical simulation of their experiment by FEM. They found that nonassociated flow rule and strain softening were essential in localization of rupture. But in their FE analysis, rupture propagated through the sand and broke the ground surface with only a fraction of the displacement observed in experiments.

Bray et al.[6] performed FE analyses and compared the results with the clay-box experiments and anchor pull-out experiments. They showed that numerical analyses could simulate experimental results quantitatively well, provided that soil's nonlinear stress-strain relation was adequately modeled.

Tani[7] performed sandbox tests and FE analyses. He showed the importance of modeling discontinuous behavior of failure surface in analyzing the post failure process as well as the process before rupture. He showed the joint element was useful for this purpose.

In this paper, we present our sandbox test results and numerical model for simulating the test. Sandbox tests were performed to show the deformation and shear failure development in sand

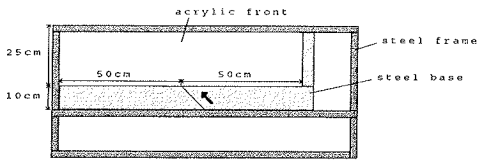

Fig.1 Apparatus for sandbox test

subjected to reverse faulting. We performed FEM analysis of our test utilizing elasto-plastic theory to model nonlinear stress-strain relation of the sand and the joint element to model failure surface of the sand. Then we apply our numerical model to prototypic real scale alluvium model calculating the dynamic movement of bedrock fault by dynamic FE analysis.

2. SANDBOX TEST

The apparatus for sandbox tests shown in **Fig.1** consisted of steel base (100 cm long and 20 cm wide) and acrylic sidewall (100cm long and 25cm high). The steel base was divided in half (50cm long). One half of them was fixed and the other half could be moved up at 45 degree relative to the fixed one. Teflon sheets were adhered on the acrylic sidewalls to reduce the friction.

Gifu sand (average grain diameter 0.33mm, uniformity coefficient 1.59[8]) was packed in the test apparatus by dropping from 1m above the base steel. Red ink-stained dry sand was added at every 3cm height as a marker. As the base fault moved up by using a hydraulic jack, the packed sand deformed and the shear failure surface developed. Typical test results are shown in **Fig.2**. **Fig.2a** shows the sand mass in the undeformed condition. The height (depth) of the sand was 17.5cm and the density computed from the total weight and the volume of the sand was 1.59g/cm^3. Shear wave velocity (110m/s) was obtained at the depth of 10cm.

The sand starts to deform in the lowest part near the base fault (**Fig.2b**). The shear failure develops upward with an increase in base displacement and it bends over to the footwall side as it approaches to the ground surface (**Fig.2c**, **Fig.2d**). The failure surface broke the ground surface when the vertical component of the base fault displacement was 8mm (4.1% of the depth of the sand). The deformation of the sand in the footwall side was observed mostly in the region near the shear failure surface and marker lines in the footwall show that they were dragged upward by the hanging wall. The deformation in the hanging wall side is small and widespread.

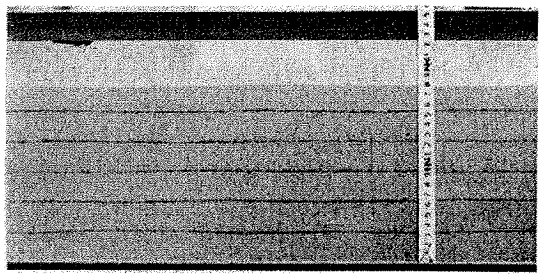

(a) initial state

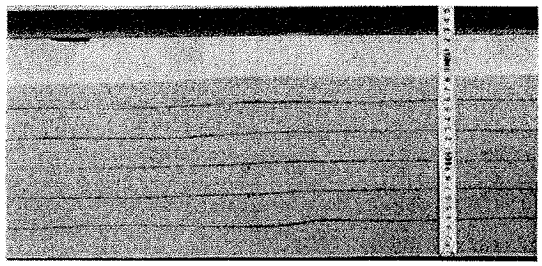

(b) vertical component of displacement 5mm

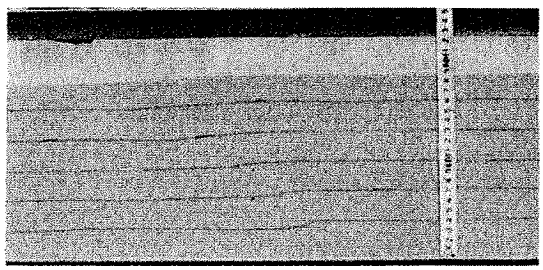

(c) vertical component of displacement 8mm

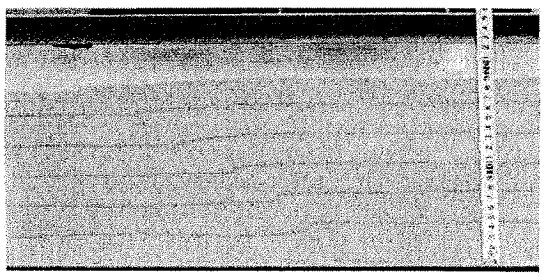

(d) vertical component of displacement 12mm

Fig.2 Deformation of sand

Once the shear failure surface reaches the ground surface, the deformation occurs mostly near this failure surface (**Fig.2d**).

For the other four experiments we performed, the same deformation pattern of the sand was observed although the location of the failure surface was slightly different from each other. The vertical component of the base fault displacement needed to break the ground surface was within the range of

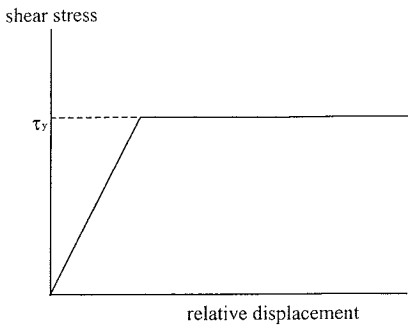

Fig.3 Constitutive relation of joint elements

7mm-9mm corresponding to 4%-5% of the depth of the sand, which is compatible with the result of Cole and Lade[1] (4%) and Tani[7] (3%-6%).

3. NUMERICAL SIMULATION OF SANDBOX TEST

(1) FEM model

We simulated our test result by FEM. Plane strain isoparametric rectangle and triangle elements were used for solid elements. The shear failure surface was modeled by joint elements (Toki and Miura[9]). Shear stress-relative displacement relation in joint elements is assumed to be elastic-perfectly plastic (**Fig.3**). The shear strength (τ_y) was obtained by Coulomb criterion. When tensile force is induced, the joint element separates and no force is transmitted. We assumed the angle of dilation was 20 degree and used observed angle of surface rupture to determine the location of failure surface based on Tani and Ueta[2].

Solid elements were modeled based on the cap model (Chen and Baladi[10]). Associated flow rule was used. In order to avoid numerical difficulties due to singularities in Mohr-Coulomb hexagonal pyramid in principal stress space, Drucker-Prager criterion was used as a failure criterion. **Fig.4** shows the FEM mesh.

(2) Parameters

Initial vertical stress (σ_v) is assumed to be ρgh, where ρ is observed density, g is the acceleration of gravity and h is the depth. Horizontal stress (σ_h) is assumed to be $\nu/(1-\nu)\sigma_v$, where ν is Poisson's ratio. Initial shear modulus (G_0) is determined as follows. Ishida et al.[8] described initial shear modulus of Gifu sand as a function of void ratio (e) and confining stress (σ_c) .

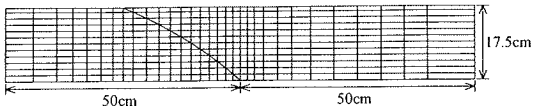

Fig.4 FEM mesh

$$G_0 = 1.42 \times 10^4 \frac{(2.17 - e)^2}{1 + e} (\sigma_c)^{0.321} \quad (1)$$

We modified equation (1) in order that the modulus calculated by equation (1) coincided with the one calculated by obtained density and shear wave velocity at the depth of 10cm.

In the Coulomb criterion, which we used for joint elements, failure is assumed to occur when the shear stress on a plane reaches a value that depends linearly on the normal stress (σ) of the plane. This is expressed as

$$\tau_y = C + \sigma \tan\phi \quad (2)$$

where τ_y is the shear strength, C and ϕ are the cohesion and angle of internal friction, respectively.

In the Drucker-Prager criterion, the failure envelope is described by (**Fig. 5**)

$$h(I_1, \sqrt{J_2}) = \sqrt{J_2} - \alpha I_1 - k \quad (3)$$

where I_1 is the first invariant of the stress tensor, J_2 is the second invariant of the deviatoric stress tensor. α and k are material constants related to the frictional and cohesive strength.

The strain hardening elliptical cap is described by

$$H(I_1, \sqrt{J_2}, \kappa) = \sqrt{J_2} - 1/R \{[X(\kappa) - L(\kappa)]^2 - [I_1 - L(\kappa)]^2\}^{1/2} \quad (4)$$

where R is the ratio of the major to the minor axis of the elliptic cap. $X(\kappa)$ and $L(\kappa)$ define the intersections of the elliptic cap with the I_1 axis and failure envelope (equation (3)), respectively. κ is the hardening parameter and is assumed to be

$$\kappa = \varepsilon_{kk}^p = W\{1 - \exp[-DX(\kappa)]\} \quad (5)$$

where ε_{kk}^p is the plastic volumetric strain, W and D are material constants.

Tatsuoka et al.[11] showed that the change of the deformation characteristics of Toyoura sand with the change of σ_3 was rather small when σ_3 is lower than around 49kPa.

Plane strain tests were performed under σ_3=49kPa to determine parameters. Internal friction angle of joint elements was obtained by the peak stress. Cohesion is assumed to be 0Pa. Parameters of the cap model were determined by trial and error so that the calculated stress-strain curve fitted the curve obtained by the plane strain tests. Parameters used in our numerical analysis are listed in **Table1**.

Table 1 Parameters of numerical analysis

			Solid element	Joint element
Initial shear modulus		G_0	Equation (4)	Equation (4)
Poisson's ratio		ν	0.3	
Density			$1.59g/cm^3$	
Parameters of Mohr-Coulomb criterion	Cohesion	C		0.0Pa
	Friction angle	ϕ		51.4 degree
Parameters of Drucker-Prager criterion		α	0.27	
		k	0.0Pa	
Hardening function parameters		D	$0.002(kN/m^2)^{-1}$	
		W	0.15	
Major axis/minor axis		R	3.1	

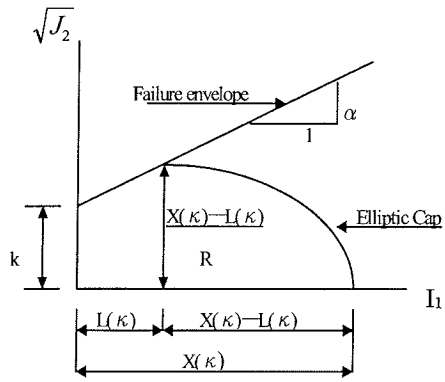

Fig.5 Yield surfaces and parameters of functions

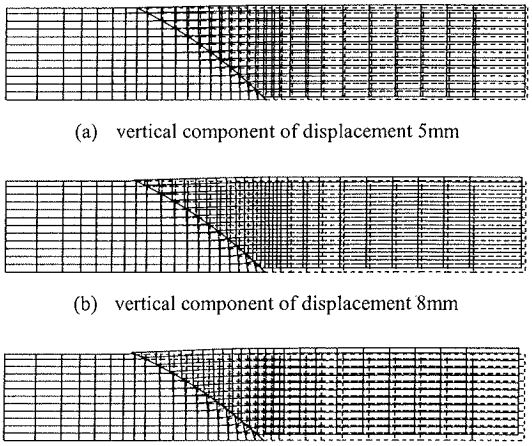

(a) vertical component of displacement 5mm

(b) vertical component of displacement 8mm

(c) vertical component of displacement 12mm

Fig.6 Result of FEM analysis

(3) Result

Fig.6 shows the calculated deformation of the sand when the vertical component of the base fault displacement was 5mm (**Fig.6a**), 8mm (**Fig.6b**) and 12mm (**Fig.6c**). In **Fig.6a**, relatively large deformation is observed in the lower region near the base fault, while the deformation near the ground surface is small and widespread. When the base fault displacement increases, we can distinguish the slip between the hanging wall and the footwall. In **Fig.6b**, slip can be seen in all joint elements. After formulating distinct slip throughout the sand, base fault displacement was consumed mostly by the slip in joint elements (**Fig.6c**).

The joint element at the ground surface ruptured when the vertical component of the base fault displacement was 3.2mm. The relative vertical displacement of the joint element is less than 0.04mm in this case. When the vertical displacement of the base fault is 7mm, the relative vertical displacement of the joint element at the ground surface exceeds 1mm and the slip becomes distinct. This value is compatible with the result of our test (8mm).

The deformation of solid elements is large in the lower part near the failure surface of the footwall and small in the hanging wall side. The solid elements in the footwall side are dragged upward by the hanging wall. These two are compatible with the experimental result.

The slip in failure surface (joint elements) is large in shallow part compared to the test. This may be because we neglected the width of joint elements in our simulation while the shear failure surface has a certain width in real sand.

Our simulation can duplicate the test results generally well including the process of formulating shear failure surface and the process after it.

4. APPLICATION OF NUMERICAL MODEL TO PROTOTYPIC REAL SCALE ALLUVIUM

(1) Method

We applied our numerical model to the prototypic real scale sandy alluvium and investigated the dynamic failure propagation in the alluvium. Our numerical analyses were divided into two parts. First, assigning dynamic rupture parameters on the bedrock fault, the dynamic movement of the bedrock fault was calculated[9),12)]. Then applying the obtained dynamic bedrock fault movement to the alluvium as a boundary condition, the failure process of the alluvium was calculated.

(2) Analysis of the bedrock fault

We used plane strain isoparametric rectangle and triangle elements and joint elements for the analysis of the bedrock fault. The joint elements are arranged along a potential fault plane. The assumed shear stress-relative displacement relation of joint elements in the bedrock is shown in **Fig.7a**. In **Fig.7a**, τ_0 and τ_d are the initial and the residual stress, respectively. The strength excess is defined as the difference between the shear strength and the initial stress. The stress drop is defined as the difference between the initial stress and the residual stress. The shear stress-relative displacement relation of a joint element in the alluvium is assumed to be elastic-perfectly plastic (**Fig.7b**).

Fig.8 shows the FEM mesh. The dip angle of the fault is assumed to be 45 degree. The model consists of two layers. The upper one (100m) is the alluvium layer and the lower one (19.2km) is the bedrock layer. The density along with S wave velocity and Poisson's ratio of each layer are listed in **Table 2**.

To eliminate artificial reflections, we adopted absorbing boundary conditions[13)]. We used the Reyleigh type damping matrix written as follows,

$$[c] = 1.4h\omega_1[m] + 0.6\frac{h}{\omega_1}[k] \qquad (6)$$

where $[m]$ and $[k]$ are the mass and stiffness matrices, ω_1 is the primary natural angular frequency. The damping constant (h) in the bedrock and the alluvium were assumed to be 0.01 and 0.1, respectively.

When the shear stress in a joint element of the bedrock reaches the shear strength, it drops to the residual stress, which generates seismic wave. The shear stress in adjacent joint elements is increased by the seismic wave. If the stress in adjacent joint elements reaches the shear strength, the stress drop occurs and the rupture propagates. On the other hand, if the strength excess is high and the shear stress does not reach the shear strength, the rupture stops there.

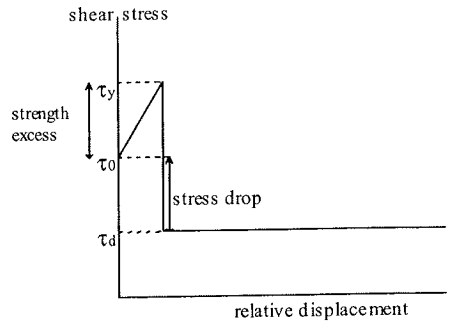

Fig.7a Stress – relative displacement relation of bedrock joint elements

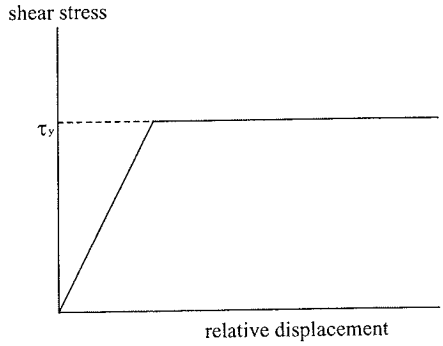

Fig.7b Stress – relative displacement relation of alluvium joint elements

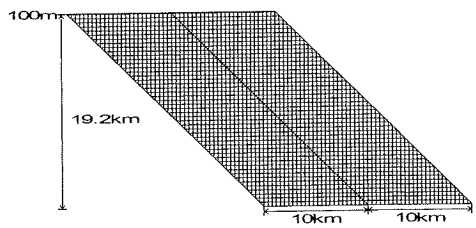

Fig.8 FEM mesh for bedrock fault analysis

Table 2 Parameters of bedrock – alluvium model

	Density	S wave velocity	Poisson's ratio
Alluvium	1.7g/cm^3	200m/s	0.3
Bedrock	2.5g/cm^3	3500m/s	0.25

Table 3 Parameters of bedrock fault and result

	Fault width	Stress drop	Strength excess	Vertical component of fault slip	Moment magnitude
Case1	19.2km	4.0MPa	4.7MPa	5.4m	7.33
Case2	19.2km	3.0MPa	4.0MPa	4.1m	7.25
Case3	19.2km	2.0MPa	2.5MPa	2.7m	7.20
Case4	19.2km	1.8MPa	2.5MPa	2.4m	7.17
Case5	19.2km	1.5MPa	2.0MPa	2.0m	7.12
Case6	9.6km	3.0MPa	4.0MPa	1.6m	6.60
Case7	9.6km	2.0MPa	2.5MPa	1.0m	6.48
Case8	9.6km	1.5MPa	2.0MPa	0.8m	6.40

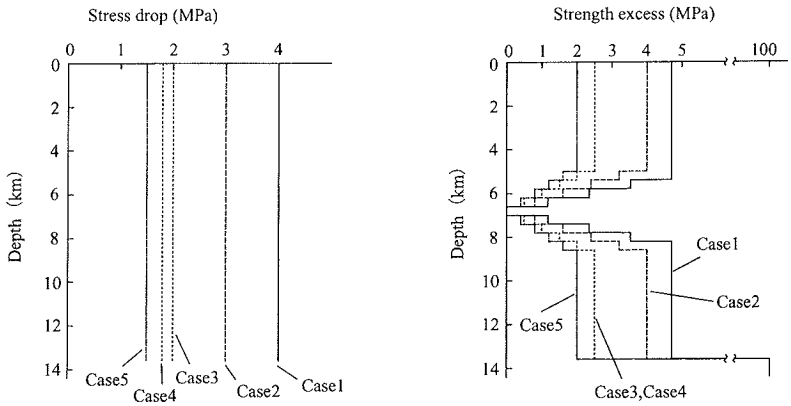

(a) from case1 to case5

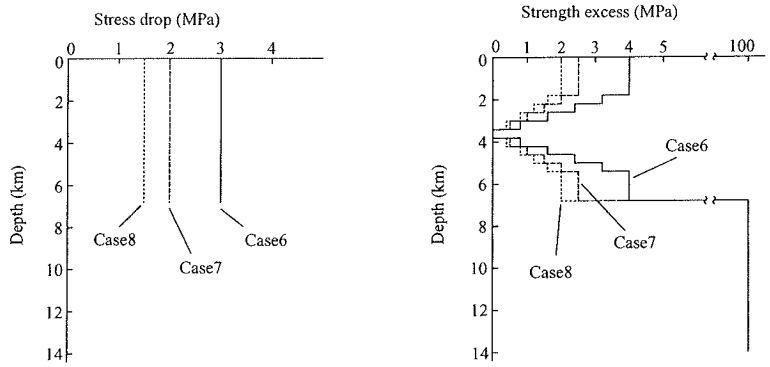

(b) from case6 to case8

Fig.9 Stress drop and strength excess

Assigning different strength excess and stress drop in each joint element, eight different bedrock fault movements were calculated (case1-case8) as shown in **Table 3**. Extremely high strength excess (100MPa) was assigned to lower joint elements and fault width was restricted to 19.2km (case 1-case 5) and 9.6km (case 6-case 8). Strength excess at the center of the presumed bedrock fault was set to 0 and the rupture propagated bilaterally from the point. The strength excess distribution on the fault was given in order that the rupture would propagate with a velocity slightly less than the S wave velocity (**Fig.9**). The stress drop on a fault was assumed to be constant in each case (**Fig.9**). The bedrock fault

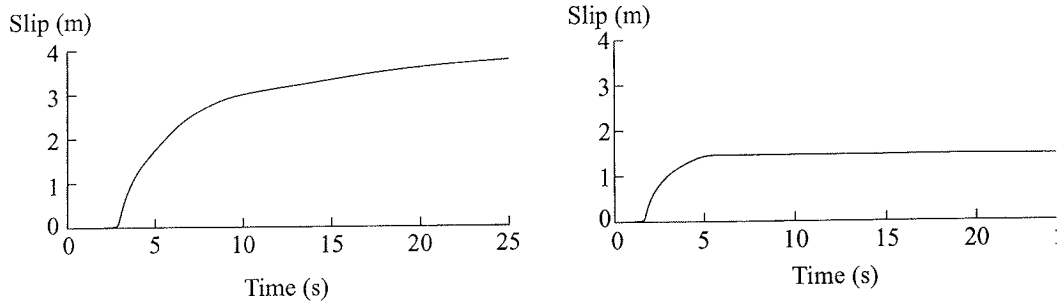

(a) case3 (b) case7

Fig.10 Source time function

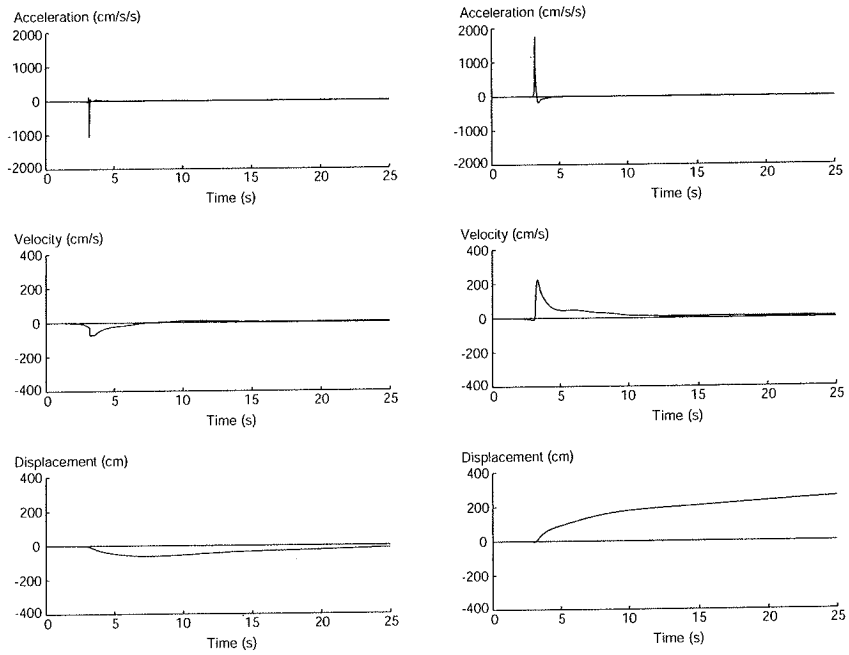

(a) horizontal component (b) vertical component

Fig.11 Deformation curve in case 4

movement was calculated for 25s with the time interval of 0.015s.

The calculated source time functions at the bottom of the alluvium layer are shown in **Fig.10**. **Fig.10a** and **Fig.10b** show the source time function in case3 and case7, respectively.

Fig.11 shows the time history of acceleration, velocity and displacement at the point beneath the alluvium on the hanging wall side of the fault. The rapid increase of acceleration and velocity is observed just after the arrival of the rupture. The acceleration decreases rapidly, while the velocity decays with time. Similar time history pattern was obtained for other cases, because similar stress drop and strength excess distribution pattern was assumed in every case.

Table 3 shows the final vertical displacement of the fault and the moment magnitude (M_w) of each earthquake. The moment magnitude was given by the relation $\log M_0 = 1.5M_w + 16.1$, where M_0 is the seismic moment and was calculated on the assumption that L (fault length) = $2W$ (fault width).

Table 4 Parameters of numerical analyses

			Solid element	Joint element
Initial shear modulus			*1)	*1)
Poisson's ratio		ν	0.3	
Density			1.7g/cm^3	
Parameters of Mohr-Coulomb criterion	Cohesion	C		0.0Pa
	Friction angle	ϕ		43.0 degree
Parameters of Drucker-Prager criterion		α	0.23	
		k	0.0Pa	
Hardening function parameters		D	0.00009(kN/m^2)$^{-1}$	
		W	0.05	
Major axis/minor axis		R	2.0	

*1) given by density and S wave velocity

(3) Analysis of the alluvium

a) Numerical model

The calculated bedrock movement was applied to the alluvium model as a boundary condition and analyzed the rupture propagation through the alluvium.

In order to investigate the effect of the depth of the alluvium, four alluvium models with the depth of 30m, 50m, 75m and 100m were used. Joint elements were arranged along the potential shear failure surface. This failure surface was determined by Tani and Ueta[2]. The FEM meshes for these models are shown in **Fig.12**. The stress–relative displacement relation of joint elements was assumed to be elastic-perfectly plastic. The solid elements were assumed to be elasto-plastic and were modeled using the cap model. Parameters of the joint elements and the cap model were determined based on the plane strain tests performed in high confining stress (σ_3=392kPa) (Park & Tatsuoka[14]) (Tatsuoka et al.[15]). Parameters used in the alluvium analyses are shown in **Table 4**.

The vertical stress in joint elements and solid elements was assumed to be ρgh. The initial horizontal stress was assumed to be proportional to the vertical stress and two different conditions (0.4 times vertical stress and 0.7 times vertical stress) were considered. The initial shear modulus was calculated by the density and shear wave velocity, and two different velocity structures of the alluvium were assumed (constant velocity model and variable velocity model shown in **Fig.13**).

We used the Reyleigh type damping matrix and the damping constant was assumed to be 0.01[16].

Applying dynamic bedrock fault movement to these alluvium models with different initial conditions, we performed the analysis of the

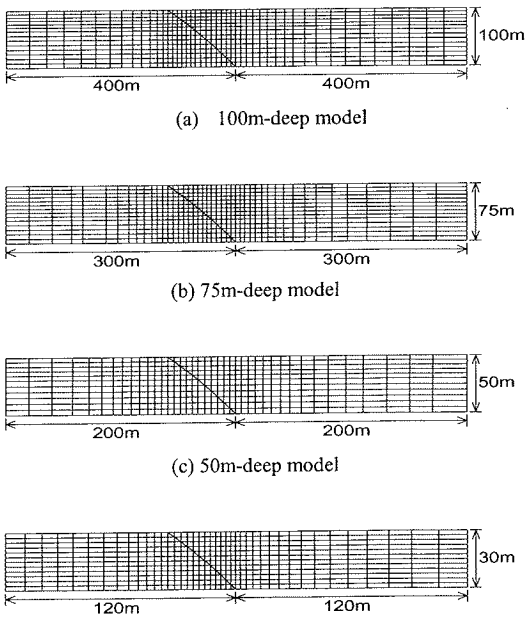

(a) 100m-deep model

(b) 75m-deep model

(c) 50m-deep model

(d) 30m-deep model

Fig.12 FEM mesh for alluvium

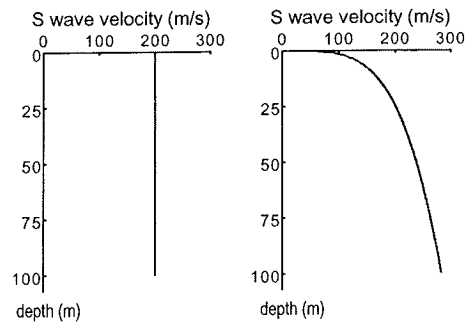

Fig.13 Assumed shear wave velocity structure of the alluvium

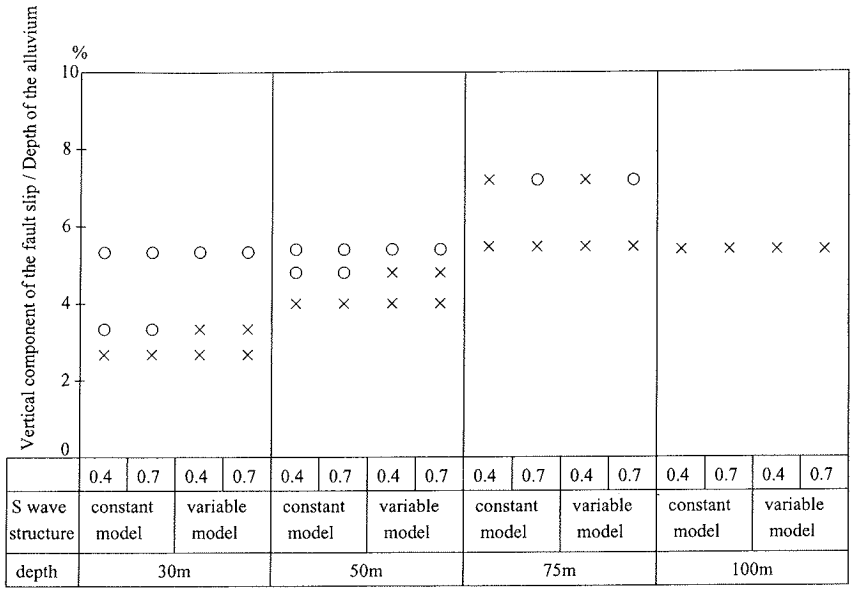

Fig.14 Result of numerical analyses

alluvium. The equation of motion of the system is written as

$$[M]\{\ddot{u}\}+[C]\{\dot{u}\}+[K]\{u\}=\{f\} \qquad (7)$$

where $[M]$, $[C]$ and $[K]$ are the mass, damping and stiffness matrices, $\{u\}$ is the nodal displacement, $\{f\}$ is the external force vector caused by the nonlinearity. Dividing nodal displacement (u) into u_1 and u_2, where u_1 and u_2 are respectively the nodal displacement inside the alluvium and on the boundary, equation (7) can be written as

$$\begin{bmatrix} M_{11} & M_{12} \\ M_{21} & M_{22} \end{bmatrix}\begin{Bmatrix} \ddot{u}_1 \\ \ddot{u}_2 \end{Bmatrix}+\begin{bmatrix} C_{11} & C_{12} \\ C_{21} & C_{22} \end{bmatrix}\begin{Bmatrix} \dot{u}_1 \\ \dot{u}_2 \end{Bmatrix}+\begin{bmatrix} K_{11} & K_{12} \\ K_{21} & K_{22} \end{bmatrix}\begin{Bmatrix} u_1 \\ u_2 \end{Bmatrix} = \begin{Bmatrix} f_1 \\ f_2 \end{Bmatrix} \qquad (8)$$

$\{u_1\}$ can be calculated from the first equation.

$$[M_{11}]\{\ddot{u}_1\}+[C_{11}]\{\dot{u}_1\}+[K_{11}]\{u_1\}= \{f_1\}-[M_{12}]\{\ddot{u}_2\}-[C_{12}]\{\dot{u}_2\}-[K_{12}]\{u_2\} \qquad (9)$$

b) Result and discussion

The shear failure propagated from lower part to upper part of joint elements. In some cases the failure propagated through the alluvium and broke the ground surface. In other cases it did not.

Fig.14 summarizes the simulation results. Open circle indicates that the shear failure occurred in all of the joint elements. Cross indicates that it did not. In 30m-deep alluvium model, all joint elements in the alluvium ruptured when the alluvium was subjected to the bedrock movement obtained in case 6. The vertical component of the bedrock fault slip is 1.6m, corresponding to 5.3% of the depth of the alluvium. In 50m-deep alluvium model, all joint elements ruptured with 2.7m vertical slip of the bedrock fault, corresponding to 5.4% of the depth of the alluvium. Some joint elements did not rupture with 0.8m vertical slip (2.7% of the depth) in 30m-deep alluvium model and 2.0m vertical slip (4% of the depth) in 50m-deep alluvium. The simulation result depends on the conditions of the alluvium when the alluvium was subjected to 1.0m vertical slip (3.3% of the depth) and 2.4m vertical slip (4.8% of the depth) in 30m and 50m alluvium model respectively. In 75m alluvium model, some joint elements did not rupture with 4.1m vertical slip of the bedrock fault (5.5% of the depth of the alluvium). When the 75m-deep alluvium was subjected to 5.4m vertical slip (7.2% of the depth of the alluvium), all joint elements ruptured in compressive initial stress state, while some joint elements did not rupture if the initial horizontal stress was assumed to be 0.4 times the vertical stress. More than 5.4m vertical slip was needed for all joint elements to rupture in 100m-deep alluvium model.

Generally the failure propagated from lower part to upper part of joint elements, however because of low confining stress the failure at the ground surface occurred due to seismic wave before the shear failure

reached to the ground. The slip in joint elements in this case was small and the slip in joint elements has become distinct after all joint elements ruptured.

Bray et al.[6] performed FEM analyses of fault rupture propagation through 23m-deep cohesive soils overlying 45 degree reverse fault, 60 degree normal fault and 90 degree reverse fault, and showed that the height of the shear rupture zone was 18-26 times the magnitude of the bedrock fault displacement with the fault rupture zone reaching the ground surface at a normalized base displacement of roughly 4%. They also showed that the normalized base displacement required to propagate the shear rupture zone to the ground surface was roughly inversely proportional to the soil's failure strain. Our results of 30m and 50m-deep alluvium models are compatible with their analyses of the 24m-deep model.

The stress-strain curve of sand expands and shifts toward higher strain side as the confining stress increases[17]. The shear failure strain becomes large with confining stress accordingly. This is the reason our numerical analyses show that more bedrock fault slip is needed to rupture joint elements for deeper alluvium model compared to the alluvium depth.

Since the rupture propagation in the alluvium over reverse fault is considered, the rupture in the alluvium is likely to occur in the compressive state of stress as shown in the 75m-deep alluvium analyses. The constant shear velocity model gives higher shear modulus on the average in 30m and 50m-deep alluvium model. The 30m and 50m-deep alluvium analyses show that higher shear modulus makes the shear failure propagate more easily if the parameters of failure criteria are assumed to be independent of the shear modulus.

All joint elements did not rupture in our 100m -deep alluvium model by the largest bedrock movement (case 1). The moment magnitude of case 1 is 7.33 and the obtained vertical slip 5.4m is large compared with its magnitude because we assumed large stress drop in the shallow part of the bedrock fault. Earthquakes of magnitude greater than 7.3 seldom occur in inland (intra plate)[18]. It is unlikely that the shear failure propagates through the 100m-deep sandy alluvium.

5. CONCLUSION

We performed sandbox tests and numerical analysis of the tests to investigate the shear failure propagation in deposits by reverse faulting. The FE analysis using elasto-plastic solid elements and joint elements to model shear failure surface can duplicate our test result generally well, if the stress-strain relation of the sand is properly modeled.

Applying the numerical model to the prototypic real scale sandy alluvium, the following conclusion has been obtained.

(1) The shear failure propagates through the sandy alluvium and breaks the ground surface if the vertical component of the bedrock fault slip reaches 3-5% of the depth of the alluvium regarding 30m and 50m-deep alluvium. For 75m-deep alluvium, vertical slip of about 7% of the depth of the alluvium is needed for shear failure to propagate through the alluvium. It is unlikely that the shear failure propagates through 100m-deep alluvium.

(2) Compressive stress state and high shear modulus appear to promote the shear failure propagation in alluvium over reverse fault, if the parameters of the failure criteria are assumed to be independent of the stress state and shear modulus.

REFERENCES

1) Cole, D.A.Jr. and Lade, P.V.: Influence zones in alluvium over dip-slip faults, *J. Geotech. Engrg*, ASCE, Vol. 110, No. 5, pp. 599-615, 1984.
2) Tani, K. and Ueta, K.: Shape and location of discontinuity in sand induced by fault displacement in bed rock, *Proc. 26 Japan National Conf. on Geotech. Engrg*, pp. 1185-1188, 1991. (in Japanese)
3) Scott, R.F. and Schoustra, J.J.: Nuclear power plant sitting on deep alluvium, *J. Geotech. Engrg*, ASCE, Vol. 100, pp. 449-459, 1974.
4) Roth, W.H., Kalsi, G., Papastamatiou, O. and Cundall, P.A.: Numerical modeling of fault propagation in soils, *Proc., 4 th Int. Conf. on Num. Meth. Geomech.*, pp. 487-494, 1982.
5) Walters, J.V. and Thomas, J.N.: Shear zone development in granular materials, *Proc. 4th. Int. Conf. Num. Meth. Goemech.*, I, pp. 263-274, 1982.
6) Bray, J.D., Seed, R.B. and Seed, H.B.: Analysis of earthquake fault rupture propagation through cohesive soil, *J. Geotech. Engrg.*, ASCE, Vol. 120, No.3, pp. 562-580, 1994.
7) Tani, K.: Numerical simulation of model test of reverse fault by FEM incorporating joint elements, *Proc. of Symposium on subsurface failure and localization of strain*, pp. 215-222, 1994. (in Japanese)
8) Ishida, T., Watanabe, H., Ito, H., Kitahara, Y. and Matsumoto, M.: Static and dynamic property of model test material (Gifu sand etc.) under low confining stress, *CRIEPI Report*, 1981. (in Japanese)
9) Toki, K. and Miura, F.: Simulation of a fault rupture mechanism by a two-dimensional finite element method, *J. Phys. Earth*, Vol. 33, pp. 485-511, 1985.
10) Chen, W.F. and Baladi, G.Y.: *Soil Plasticity*, Elsevier, 1985.
11) Tatsuoka, F., Sakamoto, M., Kawamura, T. and Fukushima, S. : Strength and deformation characteristics of sand in plane

strain compression at extremely low pressures, *Soils and Foundation*, Vol.26, No.1, pp.65-84, 1986.
12) Inoue, T: Prediction of strong motion near fault by dynamic model: Master thesis, University of Tokyo, 1996. (in Japanese)
13) Miura, M. and Okinaka, H.: Dynamic analysis method for 3-D soil-structure interaction system with the viscous boundary based on the principle of virtual work, *Proc. of JSCE*, Vol. 404/I-11, pp. 395-404, 1989. (in Japanese)
14) Park, C.S., and Tatsuoka, F.: Anisotropic strength and deformation of sands in plane strain compression, *Proc. XIII ICSMFE*, Vol. 1, pp.1-4, 1994.
15) Tatsuoka, F., Goto, S., Siddiquee, M.S.A., Yoshida, T., Kihata, Y. and Sato, T.: Deformation and strength characteristics of SLB sand and model testing method for Class-A prediction of model bearing capacity tests using a strip footing, *Proc. of Symposium on subsurface failure and localization of strain*, pp. 1-8, 1994. (in Japanese).
16) Ohshima, Y. and Watanabe, H.: An elasto-plastic dynamic response analysis of underground structure-soil composite based upon the 3-d finite element method, *Proc. of JSCE*, No.495/I-28, pp.31-42, 1994.
17) Ishihara, K.: *Soil Behavior in Earthquake Geotechnics*, Oxford Science Publication, 1996.
18) Asada, T.: Some questions of active faults, *Active Fault Research*, Vol. 9, pp. 1-3, 1991.

(Received September 3, 2001)